

# Dual-Channel Single-Molecule Fluorescence Resonance Energy Transfer to Establish Distance Parameters for RNA Nanoparticles

Dan Shu,<sup>†,||</sup> Hui Zhang,<sup>†,||</sup> Roman Petrenko,<sup>‡</sup> Jarek Meller,<sup>§</sup> and Peixuan Guo<sup>†,\*</sup>

<sup>†</sup>Nanobiomedical Center, College of Engineering and Applied Science/College of Medicine, University of Cincinnati, Cincinnati, Ohio 45221, United States, <sup>‡</sup>Department of Physics, and <sup>§</sup>Department of Environmental Health, University of Cincinnati, Cincinnati, Ohio 45267, United States. <sup>||</sup>These authors contributed equally to this work.

The emergence of RNA nanotechnology has necessitated imaging systems with nanometer-scale resolution for RNA studies. The resolution power of conventional optical microscopy is limited by light diffraction. The resolution limit in optical microscopy can be estimated as  $1.22\lambda/(2NA)$ ;  $\lambda$  denotes the wavelength of the light detected; NA denotes the numerical aperture of the objective used. Thus, the larger the NA, the higher the resolution. With a 1.3 or 1.4 NA lens, the resolution equals approximately half of the wavelength. To reduce background noise, enhance sensitivity, and improve resolution, methods such as single-molecule detection,<sup>1</sup> combined with photobleaching,<sup>2–5</sup> fluorescence resonance energy transfer (FRET),<sup>6–8</sup> FRET correlation spectroscopy,<sup>9</sup> and nanometer localization<sup>10–13</sup> have been developed. Optical devices and mechanical probes sensitive enough to measure single molecules have brought about a new era in RNA research. Single-molecule approaches allow for direct observation of physical behavior and provide answers to many questions, including how RNA molecules fold into 3D structures, how they interact to assemble quaternary complexes, and how conformational changes are related to the production of force.

In single-molecule FRET (smFRET) studies, a laser is used to excite the donor fluorophore (Cy3, for example), which will emit fluorescence with a range of defined wavelength. When an acceptor (Cy5, for example) is located at a distance within 10 nm from the donor, the energy will be transferred to the acceptor, which would fluoresce due to this transfer. In this case,

**ABSTRACT** The increasing interest in RNA nanotechnology and the demonstrated feasibility of using RNA nanoparticles as therapeutics have prompted the need for imaging systems with nanometer-scale resolution for RNA studies. Phi29 dimeric pRNAs can serve as building blocks in assembly into the hexameric ring of the nanomotors, as modules of RNA nanoparticles, and as vehicles for specific delivery of therapeutics to cancers or viral infected cells. The understanding of the 3D structure of this novel RNA dimeric particle is fundamentally and practically important. Although a 3D model of pRNA dimer has been proposed based on biochemical analysis, no distance measurements or X-ray diffraction data have been reported. Here we evaluated the application of our customized single-molecule dual-viewing system for distance measurement within pRNA dimers using single-molecule Fluorescence Resonance Energy Transfer (smFRET). Ten pRNA monomers labeled with single donor or acceptor fluorophores at various locations were constructed and eight dimers were assembled. smFRET signals were detected for six dimers. The tethered arm sizes of the fluorophores were estimated empirically from dual-labeled RNA/DNA standards. The distances between donor and acceptor were calculated and used as distance parameters to assess and refine the previously reported 3D model of the pRNA dimer. Distances between nucleotides in pRNA dimers were found to be different from those of the dimers bound to procapsid, suggesting a conformational change of the pRNA dimer upon binding to the procapsid.

**KEYWORDS:** DNA packaging motor · RNA 3D structure · nanotechnology · nanobiotechnology · nanomedicine · distance measurement of nanoparticles

there is an observable drop in fluorescence intensity that corresponds to the donor wavelength and a consequent increase in acceptor intensity. The transfer of energy is a nonradiative, long-range, dipole–dipole coupling process.<sup>14</sup> The efficiency of energy transfer is highly related to the distance between the FRET pair. It has been demonstrated by measurements of dsDNA rulers that FRET efficiencies are distance dependent and follow the Förster theory.<sup>15–17</sup> FRET studies on tRNA<sup>18</sup> were consistent with data from structure studies by X-ray crystallography.<sup>19</sup> Ha and co-workers monitored the conformational changes of 16S rRNA by smFRET.<sup>20</sup> SmFRET has also been successfully used in ribozyme kinetic studies.<sup>21–23</sup> However, the practice of smFRET in

\*Address correspondence to guopn@ucmail.uc.edu.

Received for review June 30, 2010 and accepted October 04, 2010.

Published online October 18, 2010. 10.1021/nn1014853

© 2010 American Chemical Society

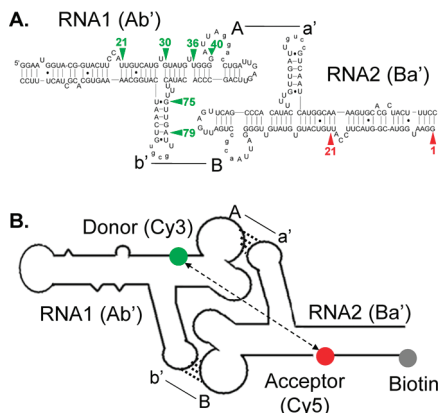


**Figure 1.** Illustration of (A) sequence and (B) structure of the pRNA dimer. The same letters in upper and lower case indicate complementary sequences for the pRNA loop/loop interaction, while different letters indicate noncomplementary loops. For example, pRNA Ab' represents pRNA where right loop A (5'G45G46A47C48) is complementary to left loop a' (3'C85C84U83G82) of pRNA Ba'; and left loop b' (3'U85G84C83G82) is complementary to right loop B (5'A45C46G47C48). The RNA1 and RNA2 were assembled into dimer *via* the interlocking loops. Numbers in green represent the six donor positions in subunit Ab' and numbers in red represent the two acceptor positions in subunit Ba' in two different dimers (see Table 2).

structural analysis is still challenging due to the signal instability, the fluctuation of the labels, the uncertainty of the fluorophore tethered arm size,<sup>15–17</sup> the distance limit of the FRET,<sup>24</sup> the sensitivity of the instrument, and the quenching of the fluorophore. Bioinformatic analysis has been developed for sequence and structural comparisons for RNA.<sup>25</sup> 3D modeling based on biochemical studies indicated a different topology between the ribozyme GIR1 and group I ribozymes, which can be related to their different catalytic functions.<sup>26</sup>

The mechanism of viral DNA packaging and ejection has been of great interest and been studied intensively.<sup>9,27–30</sup> Bacteriophage phi29 DNA-packaging motor contains a hexameric pRNA ring. The pRNA molecule contains two hand-in-hand interlocking loops, identified as the right- and left-hand loops marked as an upper- and a lower-case letter, respectively (Figure 1). It has been shown that there are two functional domains in pRNA — one (bases 23–97 at the central region) for intermolecular interaction and formation of the pRNA multimers, the other for DNA packaging.<sup>31–35</sup> Dimeric or trimeric pRNA have been demonstrated as the building blocks in pRNA hexamer assembly,<sup>36</sup> and can be constructed for applications in nanotechnology. The pRNA dimers or trimers derived from the phi29 pRNA system have been demonstrated as polyvalent vehicles for delivery of a variety of therapeutic molecules such as siRNA, ribozymes, or aptamers to specific cells *via* ligand directed specific targeting.<sup>37,38</sup> Further application in nanotechnology and nanomedicine will require elucidation of the 3D structure of the pRNA dimer.

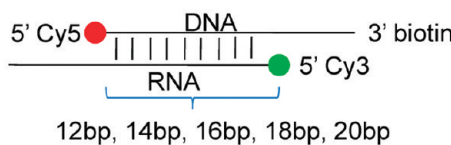
Computer modeling of the 3D structure of pRNA monomer, dimer, and hexamer has been reported.<sup>39</sup> Generation of these models was based on indirect methods including photoaffinity cross-linking,<sup>32,40–42</sup> chemical modification interference,<sup>43,44</sup> complementary modification,<sup>33,45,46</sup> cryo-AFM,<sup>36,43,44,47</sup> mutagenesis,<sup>33,35,46,48,49</sup> ribonuclease probing,<sup>31,41</sup> primer extension,<sup>41</sup> and oligo targeting.<sup>50,51</sup> Recently, our lab has assembled a customized single-molecule dual-viewing TIRF imaging system (SMDV-TIRF) with single fluorophore sensitivity and dual-color imaging ability.<sup>4,52,53</sup> In this report, we evaluate its efficacy to establish more accurately measured distance parameters for the pRNA dimer based on the results from single-molecule FRET, for refinement of the 3D model.

## RESULTS AND DISCUSSION

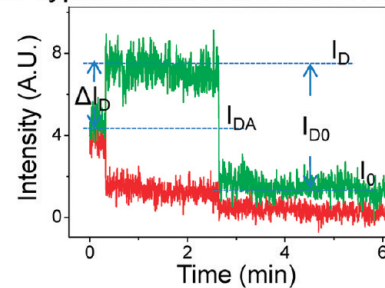
**Determination of the Arm Length of the Fluorophores.** The distance range between the donor and the acceptor to achieve measurable energy transfer is approximately 1–7.5 nm for a Cy3/Cy5 pair.<sup>24</sup> The labeling of RNA with fluorescent dyes generates tethered arms whose length is an important factor in distance determination by FRET. However, it is difficult to obtain a solid value of arm size for each fluorophore due to other factors such as orientation, folding and flexibility in molecular arrangement. Empirical determination is one feasible approach to estimate the length for both the donor and acceptor arms. Hence, we used five standard RNA/DNA hybrids with known distances between the donor and acceptor (12bp, 14bp, 16bp, 18bp, and 20bp) (Figure 2A) to determine the empirical arm size of the fluorophore and to evaluate the feasibility of using our dual-viewing single molecule imaging system to study pRNA structure. The RNA/DNA hybrids were chosen here as the labeled pRNA dimers studied in this report were partially constructed through RNA/DNA annealing.

The FRET pair Cy3(green)/Cy5(red) (Figure 2A) was selected because of its fluorescence stability. A 532 nm green laser was used for Cy3 excitation. Both donor and acceptor signals were recorded simultaneously during continuous Cy3 excitation using the SMDV-TIRF dual channel imaging system constructed in the lab.<sup>4,52,53</sup> A typical time trajectory of fluorescence intensity for a FRET event is shown in Figure 2B. The Cy5 was photobleached before Cy3 due to its less stability, and the intensity of Cy3 increased due to the loss of FRET. The FRET event can therefore be confirmed based on a sudden drop in acceptor intensity accompanied with a sudden increase in donor intensity: in another words, the anticorrelated donor and acceptor signals. Changes of donor fluorescence intensity in the presence ( $I_{DA}$ ) and absence ( $I_D$ ) of the acceptor were measured. The FRET efficiency ( $E$ ) can be obtained based on the change of donor emission in the presence ( $I_{DA}$ ) and absence ( $I_D$ ) of the acceptor eq 1 (Figure 2B).<sup>52–55</sup>

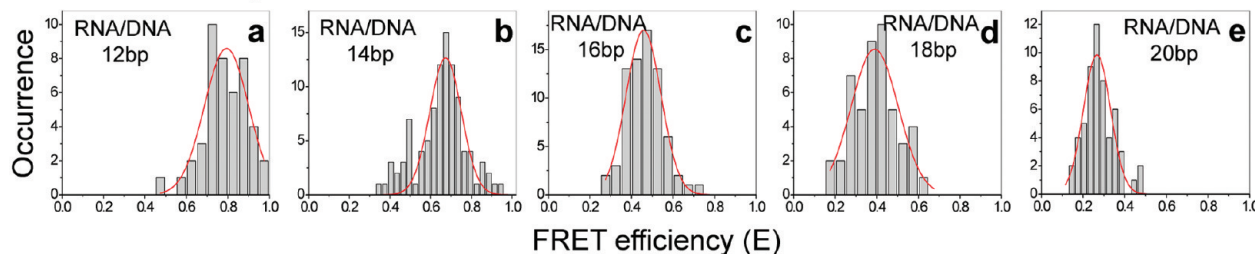
### A. Design of standard RNA/DNA hybrids



### B. Typical trace of a FRET event



### C. FRET efficiency



### D. Calculated distance

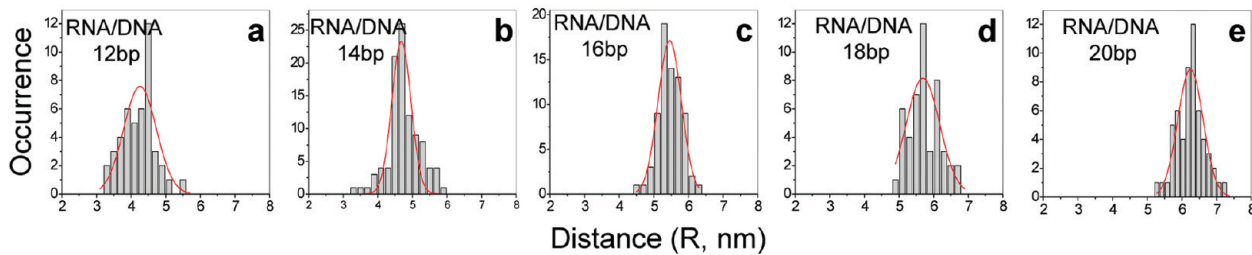


**Figure 2.** Standard distance determination of dual-labeled RNA/DNA hybrids. (A) Design of the dual-labeled RNA/DNA hybrids with different lengths of 12, 14, 16, 18, and 20 bp between Cy3 and Cy5. (B) Typical time trajectory of fluorescence intensity for a FRET event. (C) Histograms summarizing FRET efficiencies of RNA/DNA hybrids 12, 14, 16, 18, and 20 bp (a–e), respectively. (D) Histograms summarizing calculated distances of RNA/DNA hybrids 12, 14, 16, 18, and 20 bp (a–e), respectively, from FRET efficiency.

$$E = \frac{\Delta I_D}{I_{D0}} = \frac{(I_D - I_{DA})}{(I_D - I_{0Cy3})} \quad (1)$$

Unlike FRET efficiency calculations using acceptor emission,<sup>15,24,56</sup> this equation does not need to take into account of factors such as the leakages of Cy3 signal to Cy5 channel, direct excitation of Cy5 by Cy3 excitation wavelength, the different quantum yields and detection efficiency for Cy3 and Cy5, and thus simplifies the calculation. The distance ( $R$ ) between the FRET pair was derived from  $E$  by eq 2:

$$R = R_0(1/E - 1)^{1/6} \quad (2)$$

The Förster distance  $R_0$  was experimentally measured to be 5.3 nm for the Cy3/Cy5 pair, in agreement with published result.<sup>57</sup>

The FRET efficiency ( $E$ ) and distance ( $R$ ) deduced from  $E$  for each of the individual molecules were summarized in histograms (Figure 2C and D) and fitted with a Gaussian curve to obtain the mean value of  $E$  and  $R$  for each hybrid (Figure 2C and D, Table 1).

The RNA backbone contains ribose rather than the deoxyribose found in DNA. Unlike DNA, RNA is unable to coil into the B-Type double helix because the hydroxyl group at the 2'-carbon of the sugar ring in RNA makes the ring too large to fit into the allotted space for the B-Type duplex due to steric hindrance.<sup>58</sup> Therefore,

**TABLE 1. Data for the Evaluation of Arm Sizes of the Donor and Acceptor Fluorophores within Individual RNA/DNA Hybrid**

length of RNA/DNA hybrids	number of spots analyzed (N)	FRET efficiency (E)	distance (nm)	$N \times 0.275$ nm	arm size (nm)
12bp	45	$0.79 \pm 0.11$	$4.3 \pm 0.5$	3.3	1.0
14bp	99	$0.67 \pm 0.05$	$4.7 \pm 0.2$	3.9	0.8
16bp	72	$0.46 \pm 0.08$	$5.5 \pm 0.3$	4.4	1.1
18bp	48	$0.39 \pm 0.10$	$5.7 \pm 0.5$	5.0	0.7
20bp	56	$0.26 \pm 0.06$	$6.3 \pm 0.3$	5.5	0.8

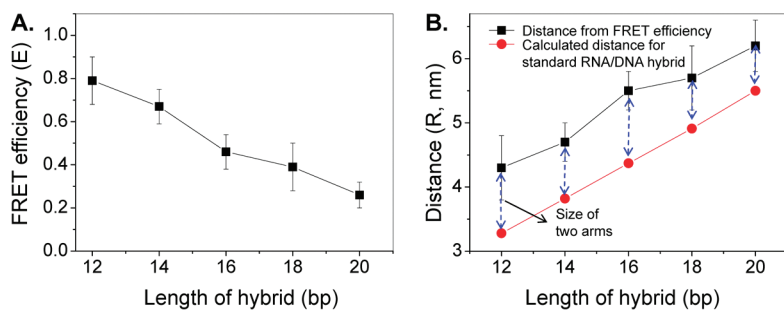


**Figure 3.** Empirical determination of the arm size of two fluorophores serving as donor and acceptor. (A) Relationship of FRET efficiencies and numbers of basepairs between the FRET pair. The error bars are the standard deviations of the measurements. (B) Comparison of empirical and theoretical distances to derive the arm size of the donor plus the acceptor fluorophores. The distances derived from FRET efficiency (black) were correlated with the theoretical distances (red) calculated from the value of 0.275 nm per rise of one basepair. The blue dotted lines indicate the empirical arm sizes for donor plus acceptor obtained from the differences.

double-stranded RNA molecules form either an A-helix, or Z-helix with specific sequences. In RNA/DNA hybrids, both RNA and DNA polynucleotide chains resist general conversion into the B-form, but rather adopt the A-conformation.<sup>59</sup> Because of the ionic strength used in our studies (100 mM NaCl, 10 mM Mg<sup>2+</sup>, 50 mM Tris-HCl, pH 8), the RNA/DNA hybrids have the following structural parameters: 10.9 bp per helix turn, a pitch of 3.0 nm and a helix rise of 0.275 nm per bp<sup>60</sup> (<http://www.whatislife.com/reader/dna-rna/dna-rna.html>). The relationships between the *E* and *R* values, with basepair numbers are plotted (Figure 3). The calculated distances were compared with theoretical distances (number of bp multiplied by 0.275 nm) (Figure 3B). These differences were used as estimates of the arm size of the

two fluorophores (Table 1). Thus, the average arm size of 0.9 nm was applied in the distance measurement in the pRNA dimer structural studies.

**Selection of Nucleotide Positions for Fluorescence Labeling.** The feasibility of applying FRET for RNA structure studies is a case by case issue. RNAs will refold partially or completely when a new chemical group, dye or nucleotide is introduced into the RNA sequence. It is not feasible to simply introduce a pair of dyes to the RNA and measure the FRET to derive the distance. However in this work, after each dye introduced into each pRNA molecule, we assess their structures and folding by at least one of the following approaches: 1. dimer formation;<sup>36,61</sup> 2. procapsid binding;<sup>31,62,63</sup> 3. DNA packaging activity;<sup>64,65</sup> 4. *in vitro* phi29 virion assembly activi-

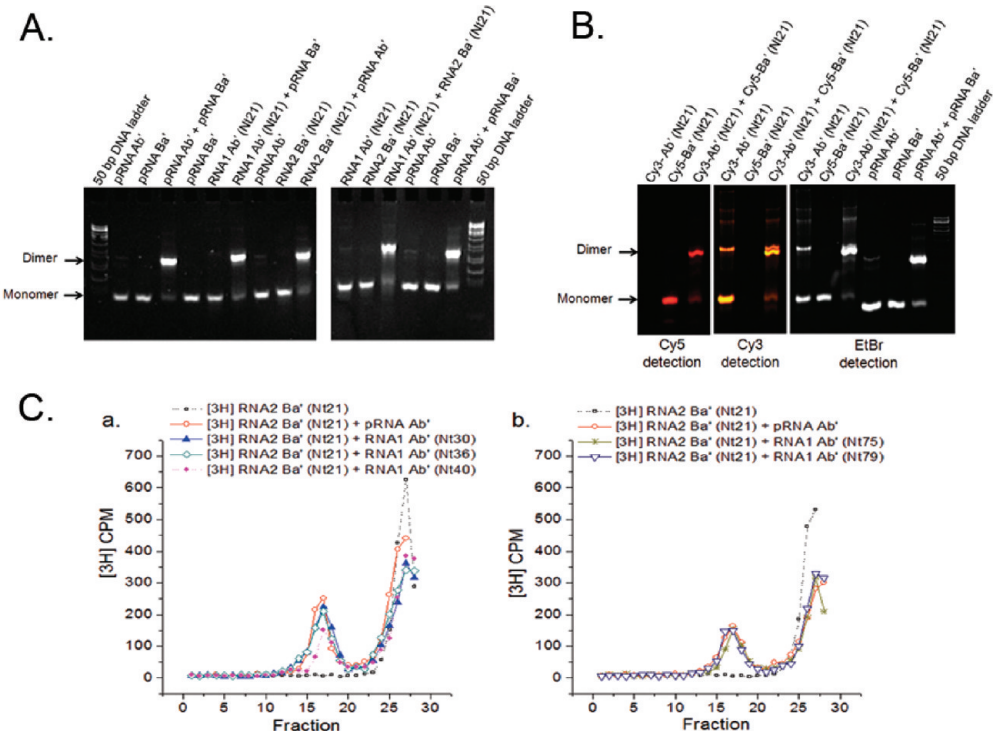


**Figure 4.** Verification of pRNA structure and function in (A–B) dimer formation and (C) procapsid binding after modification. (A) Native gel electrophoresis of modified pRNAs, compared with unmodified pRNAs. (B) Fluorescent gel images of modified pRNAs, compared with unmodified pRNAs. (C) Comparison of procapsid binding activities by [<sup>3</sup>H] counting for the modified pRNAs with unmodified pRNAs. The number of Nt indicates the position of the nucleotides for fluorescent labels.

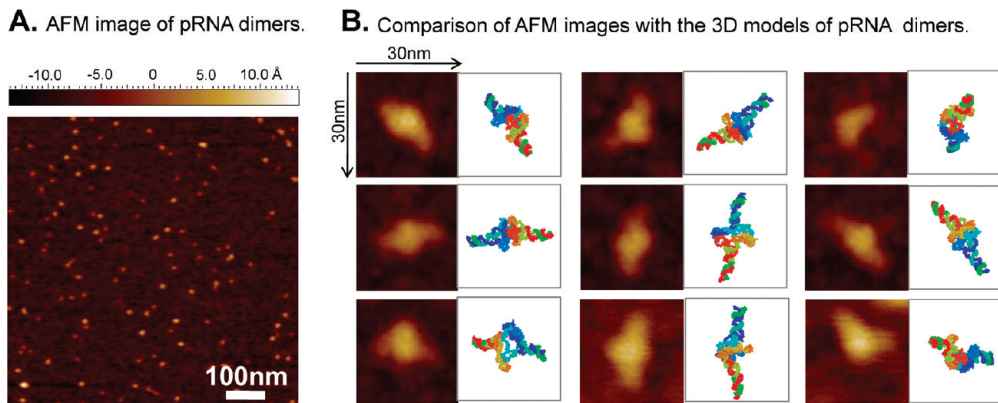


**Figure 5.** Comparison of AFM images with the 3D computer model of the pRNA dimer. (A) AFM images showing pRNA dimers. Scale bar: 100 nm. (B) Zoomed AFM images of individual pRNA dimers, compared with 3D modeling images of the pRNA dimer.

ity (Figure 4).<sup>66,67</sup> The mutated or truncated RNA with incomplete pRNA sequence would be inactive in DNA packaging or in virion assembly. Thus, using biological activity to assess their folding is not possible. In such cases, we only tested their binding to procapsid using [<sup>3</sup>H] RNA (Figure 4C). If the pRNA failed in any one of the functions, we regarded the pRNA as structurally refolded and did not consider the data comparable to the wild type pRNA.

In addition, it has been reported that FRET efficiency is affected by the orientation of the fluorophore placed in double helical nucleic acids, and a cylindrical model that accounts for the orientation factor and the helical structure has been used.<sup>15–17,68,69</sup> It is also suggested that introduction of structural flexibility for the freely rotating of the fluorophores would reduce the orientation effect.<sup>17,69</sup> In this study, we provided flexibility to the fluorophore by placing it at the terminal of the pRNA as an unfolded structure and the length of the fluorophore arm was deduced empirically with RNA/DNA hybrid standards (see first section).

**Determination of Nucleotide Distance within the pRNA Dimers.** The smFRET was utilized to obtain distances between two nucleotides (Nt) of two pRNAs in dimers (Figure 1). To simplify the description of RNA construction and multimer assembly, uppercase letters are used to represent the right-hand loop and lowercase letters to represent the left-hand loop of pRNA (Figure 1A).

The labeling of pRNA for single molecule imaging has been challenging, as single fluorophore labeling at desired nucleotide position is required. Utilizing our unique single labeling strategy coupled with the circular permutation pRNA (cpRNA) technique,<sup>48,70</sup> labeling with only one fluorophore at the desired base is ensured. The circular permutation technique generates new 3'/5' openings at desired base locations along the pRNA sequence.<sup>48,70–72</sup> The correct folding of pRNAs after this rearrangement has been extensively tested.<sup>38,48,70,73</sup> The single labeling at the new 5'-ends was then achieved by *in vitro* transcription with a fluorescent AMP.<sup>74</sup> Various RNA molecules (Figure 1B, RNA1 in the dimer) were constructed using the circular permutation pRNA approach and labeled with a single Cy3

at various nucleotides (Nt). Each labeled RNA was paired with its partner RNA2 (Figure 1B) containing both a Cy5 and a biotin moiety. The biotin label allows for immobilization to a streptavidin coated quartz slide surface for TIRF imaging. The distances between two intermolecular bases within the dimer (Figure 1B) were studied by smFRET. Dimers were assembled with high efficiency when pRNA Ab' was mixed with an equal amount of Ba', as confirmed by native PAGE gel (Figure 4A and B), procapsid binding (Figure 4C) and AFM imaging (Figure 5).

Eight partner pairs, a–h, were assembled into dimers (Table 2). Dimers a–f displayed FRET signals (Figure 6). No fluorescence energy transfer was detected for dimer g or h, indicating that the distance between the donor/acceptor pair in these dimers was out of the detectable range. This result was expected, as the data from previous 3D computer model<sup>39</sup> generated a distance of 11.1 nm between Nt1 of one pRNA and Nt21 of the second pRNA, and 9.3 nm between Nt30 of one pRNA and Nt1 of the second pRNA in the dimer. Such distances do not fall within the 1–7.5 nm range and are therefore undetectable by FRET. The calculated FRET distance included the length of the fluorophore arms. The distances after arm-size correction were used in refining the previous 3D structure of the pRNA dimer model.<sup>39</sup>

Without RNA2 (biotin-Cy5-Ba'), nonspecific binding of monomer RNA1 (Cy3-Ab') itself to the streptavidin surface was negligible, indicating that the Cy3 signals observed in our experiments were truly from the pRNA dimers. To ensure that the FRET observed was not between monomers in two adjacent dimers attached to streptavidin, a dimer composed of Cy3-Ab' and biotin-Ba', was mixed with another monomer Ba' plus monomer biotin-Cy5-Ab'. No overlapped signals of Cy3 and Cy5, and no measurable FRET were found for the mixture immobilized to the streptavidin surface. This indicates that in our experiment conditions, the possibility of two dimers or one dimer and one monomer residing close enough to produce cross FRET signals between them is very low.

**TABLE 2. Determination of Distances for 3D Modeling of pRNA Dimer**

Name of dimers	Label position		Number of spots analyzed (N)	FRET efficiency (E)	Distance (R, nm)	Distance with arm size subtracted (R, nm)	Distance from the original model (nm)	Typical FRET traces for dimers a-f	
	RNA1 (Ab')	RNA2 (Ba')						Intensity (A.U.)	Time (min)
a	30	21	125	0.46 ± 0.09	5.4 ± 0.4	4.5	4.6	Intensity (A.U.)	Time (min)
b	75	21	88	0.45 ± 0.06	5.5 ± 0.2	4.6	4.8		
c	79	21	119	0.47 ± 0.10	5.4 ± 0.4	4.5	3.7	Intensity (A.U.)	Time (min)
d	40	21	92	0.69 ± 0.09	4.7 ± 0.3	3.8	5.2		
e	36	21	109	0.51 ± 0.05	5.2 ± 0.2	4.4	3.5	Intensity (A.U.)	Time (min)
f	21	21	126	0.48 ± 0.08	5.4 ± 0.3	4.5	5.8		
g	1	21	No FRET				11.1	Intensity (A.U.)	Time (min)
h	30	1	No FRET				9.3		

**Refining the 3D Computer Model of the pRNA Dimer.** The 3D computer model of the pRNA dimer reported previously (PDB code 1L4Q)<sup>39</sup> was refined with a new set of distance parameters derived from smFRET. Explicit modeling of the fluorescent dyes Cy3/Cy5 was not feasible due to the lack of well-tested force-field parameters. Instead, harmonic parameters were applied between the backbone phosphorus atoms. Specifically, starting with the model of the pRNA dimer (PDB code 1L4Q), six distance parameters, labeled a, b, c, d, e, f (Table 2), were imposed. In addition, based on previous study,<sup>40</sup> the nucleotide 82 from one pRNA was imposed to be within 1.2 nm from nucleotides 39–41, 49, and 62–64 of the second pRNA of the dimer. Geometry optimization and further stability analysis were performed using the NAMD simulation package<sup>75</sup> for molecular dynamics, with the CHARMM27 force-field.<sup>76,77</sup> The initial structure was subjected to 10 000 conjugate-

gradient energy minimization steps with the above-mentioned parameters and a spring constant of 20 kcal/mol/Å<sup>2</sup>.

As can be seen from Figure 7A, the resulting structure that incorporates the new parameters from smFRET is qualitatively in agreement with the previously published model.<sup>39</sup> The rmsd (Root Mean Square Deviation) between the backbone atoms of the optimized structure (Figure 7A, blue) and the previous model used as the starting structure (Figure 7A, red) was 3.1 Å. The sum of squared differences (SSD) between the distances observed in the final model and the imposed distances was 107 Å<sup>2</sup>. Most of the adjustment from initial 700 Å<sup>2</sup> to the final 107 Å<sup>2</sup> occurred within the first 5000 steps of the simulations, followed by a slow decrease up to 10000 steps. To further test the sensitivity of the results, additional minimization runs with varying values of the spring constant were performed, yielding

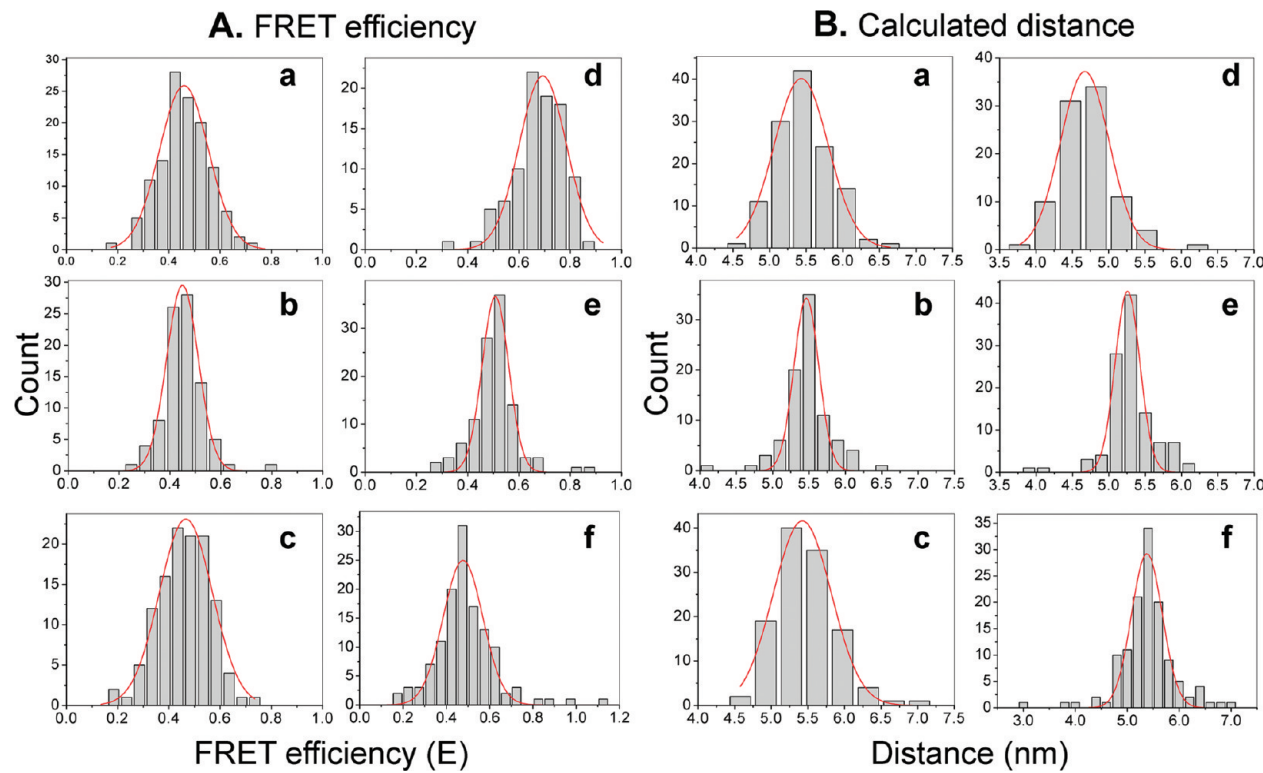


Figure 6. Distance determination of pRNA dimers corresponding to pRNA dimer a–f shown in Table 1. (A) Distribution of FRET efficiencies. (B) Summary of calculated distances of different pRNA dimers.

similar results (although more minimization steps were required for weaker harmonic parameters).

**Comparison of the pRNA Head Loop Structure in Our Published 3D Model<sup>39</sup> with a Newly Published pRNA Head Loop Structure by NMR.** An NMR structure of the pRNA head loop with base 51–61 was recently reported.<sup>78</sup> Superposition of bases

51–61 from our published computer models (yellow in Figure 8, which remained unchanged in the refined structure) with the NMR structure (PDB code 2KVN) (blue in Figure 8) revealed that the two structures agreed quite well, with a rmsd of 3.3 Å for the backbones. The differences mostly appear at positions G55,

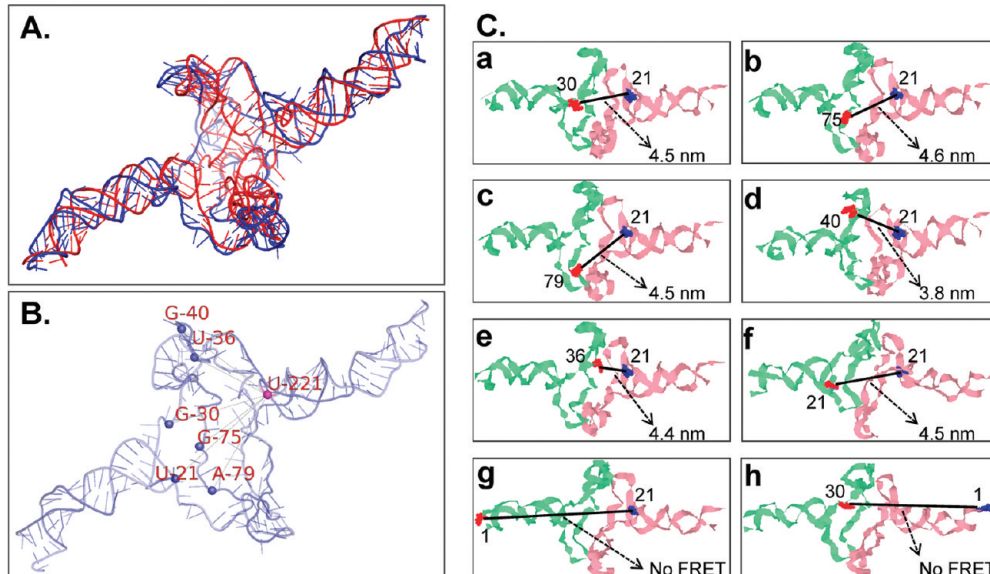
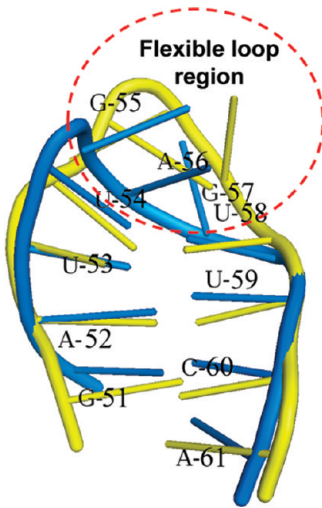


Figure 7. Refined 3D model of pRNA dimer. (A) Comparison of the original (red) and the refined (blue) models. (B) Refined structure showing positions of nucleotides used for labeling. (C) Elucidation of the location of two nucleotides that were labeled with the donor and the acceptor, respectively, in individual dimer (a–h), with one pRNA subunit in light green ribbon and the other subunit in light red. The bases used for distance measurements are in dark red spacefill format in RNA1 and blue in RNA2. Numbers represent the sequences of each nucleotide. The distances measured from FRET efficiency are indicated.



**Figure 8.** Comparison of the pRNA head loop structure in our 3D model (yellow) with a newly published pRNA head loop structure by NMR (blue). The red circle indicates the flexible loop region of the head loop structure. See Figure 1A for the complete sequence of pRNA.

A56, and G57 in the tip loop region (red circle) itself, where the structure was flexible in the NMR ensemble with a range of conformations observed. Thus, we can conclude that the refined model is consistent with the high resolution empirical ensemble within the head-loop fragment.

#### Conformational Shift of pRNA Dimer upon Binding to

**Procapsid.** It has been reported that the dimer is the binding unit of the pRNA hexamer on the procapsid.<sup>36</sup> It has also been reported that there is no pRNA sequence specificity for interaction between pRNA and the hub of the DNA-packaging motor. Instead, the specificity relies on the formation of the RNA static ring of appropriate size to fit on to the contour shape of the connector.<sup>79</sup> The mechanism in converting the dimer, which is expected to contain two closed hands, into a hexamer, which is expected to contain two open hands, is a very intriguing but still unsolved question. In comparing the FRET of labeled nucleotides in dimers to their FRET after dimer binding to the procapsid, we found a significant difference. For example, the FRET was almost undetectable in dimers composed of pRNA Ab' (Cy3 at Nt21) and Ba' (Cy5 at Nt1). However, stronger signal of Cy5 (emission around 670 nm) due to FRET was found after they bound to the procapsid (Figure 9). In another case, strong and relatively homologous FRET was detected in dimers composed of pRNA Ab' (Cy3 at Nt21)

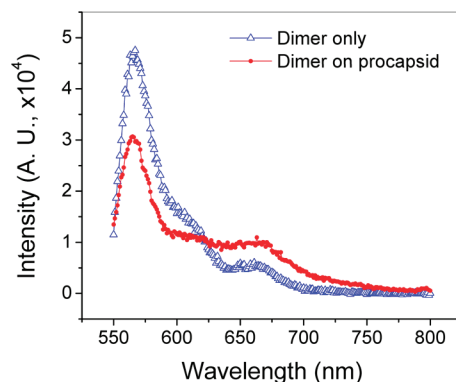


**Figure 9.** Comparison of ensemble FRET of purified dimer composed of pRNA Ab' (Cy3 at Nt21) and Ba' (Cy5 at Nt1) with that of the dimer bound to procapsid by their fluorescence emission spectra at 530 nm excitation.

and Ba' (Cy5 at Nt21), while the FRET was not assessable when they bound to the procapsid. In addition, the distance between two Nt21 in the pRNA Ab'/Ba' dimer was 5.4 nm derived from FRET. However, the distance between the Nt21s of two pRNA Ab' that bound to the procapsid is 15.4 nm as determined by Single Molecule High Resolution Imaging with Photobleaching (SHRIMP).<sup>11</sup> Due to the current impossibility of obtaining a single FRET pair in the hexamer, which is composed of three dimers, it is not possible to obtain the distance information for the hexamer using smFRET. Nevertheless, extensive studies<sup>31,36,80,81</sup> reveal that the structure of the dimer in solution is completely different from that on the procapsid, suggesting a significant conformational change upon binding to the procapsid.

#### CONCLUSION

Our previous 3D structure was derived using data obtained from multiple experiments, including photo-affinity cross-linking,<sup>32,40–42</sup> chemical modification interference,<sup>43,44</sup> complementary modification,<sup>33,45,46</sup> cryo-AFM,<sup>36,43,44,47</sup> mutagenesis,<sup>33,35,46,48,49</sup> ribonuclease probing,<sup>31,41</sup> primer extension,<sup>41</sup> and oligo targeting.<sup>50,51</sup> In this report, smFRET was used for the first time to determine the pRNA distance parameters and to enable further refinement of the 3D structure of the pRNA. The results reported here support the conclusion that smFRET data can be successfully used as a basis for deriving a high resolution 3D model of pRNA and that the previous low-resolution pRNA model is consistent with the new smFRET distance constraints.

#### METHODS

**Preparation of Dual-Labeled RNA/DNA Hybrids.** RNA oligos of different lengths with 5' Cy3 label were made by *in vitro* transcription using ADO F550/570 AMP, similar as described before.<sup>34,74</sup> The Cy3 RNA oligos were then annealed with a complementary biotin-Cy5-DNA oligo (IDT) to form RNA/DNA hybrids with different lengths between the Cy3 and Cy5 pair.

**In vitro Synthesis of Fluorescent pRNA.** To achieve single fluorophore labels at the desired positions on RNA1 in the dimer, the circu-

lar permutation strategy was applied to give a new 5' opening site at different locations.<sup>70</sup> Cy3-labeling at the 5' end of RNA was achieved by *in vitro* transcription with T7 RNA polymerase using dsDNA templates containing the T7 class II promoter ( $\varnothing 2.5$ ) in the presence of 2 mM ADO F550/570 AMP (AdeGenix, Inc.).<sup>74,82</sup> RNA2 of the dimer was made by the hybridization of a reconstructed pRNA molecule with a biotin-Cy5-DNA oligo, resulting in a label at either the corresponding nucleotide 21 or at nucleotide 1 on the pRNA molecule.

**Constructs of pRNA Dimers.** The pRNA dimers were constructed by mixing the paired pRNA molecules (Ab' and Ba') at equal concentrations in the presence of 10 mM Mg<sup>++</sup>.

**Single Molecular FRET Assay.** Streptavidin coated chamber was prepared by incubation of the quartz chamber with 1 mg/mL biotin-BSA (Sigma) for 15 min, and subsequently 0.33 mg/mL streptavidin (Prozyme) for 15 min. The biotin-labeled samples were immobilized to the chamber surface through streptavidin–biotin linkage with concentrations adjusted to give discrete fluorescent spots. Excess sample was flushed out of the chamber before imaging. A 532 nm green laser with a power of 5 mW was used for the excitation of Cy3. A 60× objective (NA = 1.4, oil immersion) was used for single fluorophore imaging. The focused beam was approximately 150 μm × 50 μm. Fluorescence signals were collected through the objective and split to Cy3 and Cy5 channels through a Dual-View imager (Optical Insights, LLC), with a dichroic (Chroma, 630Dcxr) to split Cy3 and Cy5 signals and bandpass filters for Cy3 (Chroma, D585/30 m) and Cy5 (Chroma, D680/30 m). The signals were recorded using Andor iXon 887 V electron multiplied camera. To prevent fast photobleaching, the flow cell was infused with an oxygen scavenger system (0.5% β-D-glucose, 10 mM β-mercaptoethanol, 0.2% Glucose Oxidase (Roche), and 0.25% Catalase (Sigma)) during imaging. The concentration of the samples was adjusted to show discrete fluorescing spots in the images. Sequential images were taken with an exposure time of 300 ms continuously. The recorded movie, with more than 2000 frames, was analyzed by Kinetic Imaging (Andor Technology).

**Atomic Force Microscopy Imaging.** The pRNA dimer was purified by native polyacrylamide (PAGE) gel electrophoresis and the AFM imaging of pRNA dimer was carried out as previously reported.<sup>47</sup>

**Native Gel Electrophoresis and Binding Assay of Modified pRNAs to Procapid.** The native PAGE gel electrophoresis for dimer detection followed the reported procedure.<sup>45</sup> The assay of the modified pRNA binding to procapid was performed as previously published.<sup>41</sup>

The PDB code of the original 3D model of the dimer in Protein Data Bank is 1L4Q. The refined model is available at <http://www.eng.uc.edu/nanomedicine/peixuanguo/dimer.html>.

**Acknowledgment.** We thank Anne Vonderheide for her insightful comments on the manuscript. This work was mainly supported by National Institutes of Health [grant number R01-GM059944 (PG)].

## REFERENCES AND NOTES

- Weiss, S. Fluorescence Spectroscopy of Single Biomolecules. *Science* **1999**, *283*, 1676–1683.
- Leake, M. C.; Chandler, J. H.; Wadham, G. H.; Bai, F.; Berry, R. M.; Armitage, J. P. Stoichiometry and Turnover in Single, Functioning Membrane Protein Complexes. *Nature* **2006**, *443*, 355–358.
- Shu, D.; Zhang, H.; Jin, J.; Guo, P. Counting of Six pRNAs of Phi29 DNA-Packaging Motor With Customized Single Molecule Dual-View System. *EMBO J.* **2007**, *26*, 527–537.
- Zhang, H.; Shu, D.; Huang, F.; Guo, P. Instrumentation and Metrology for Single RNA Counting in Biological Complexes or Nanoparticles by a Single Molecule Dual-View System. *RNA* **2007**, *13*, 1793–1802.
- Das, S. K.; Darshi, M.; Cheley, S.; Wallace, M. I.; Bayley, H. Membrane Protein Stoichiometry Determined From the Step-Wise Photobleaching of Dye-Labelled Subunits. *ChemBioChem* **2007**, *8*, 994–999.
- Myong, S.; Bruno, M. M.; Pyle, A. M.; Ha, T. Spring-Loaded Mechanism of DNA Unwinding by Hepatitis C Virus NS3 Helicase. *Science* **2007**, *317*, 513–516.
- Zhuang, X.; Kim, H.; Pereira, M. J. B.; Babcock, H. P.; Walter, N. G.; Chu, S. Correlating Structural Dynamics and Function in Single Ribozyme Molecules. *Science* **2002**, *296*, 1473–1476.
- Rueda, D.; Bokinsky, G.; Rhodes, M. M.; Rust, M. J.; Zhuang, X.; Walter, N. G. Single-Molecule Enzymology of RNA: Essential Functional Groups Impact Catalysis From a Distance. *Proc. Natl. Acad. Sci. U.S.A.* **2004**, *101*, 10066–10071.
- Sabanayagam, C. R.; Oram, M.; Lakowicz, J. R.; Black, L. W. Viral DNA Packaging Studied by Fluorescence Correlation Spectroscopy. *Biophys. J.* **2007**, *93*, L17–L19.
- Yildiz, A.; Forkey, J. N.; McKinney, S. A.; Ha, T.; Goldman, Y. E.; Selvin, P. R. Myosin VI Walks Hand-Over-Hand: Single Fluorophore Imaging With 1.5-Nm Localization. *Science* **2003**, *300*, 2061–2065.
- Gordon, M. P.; Ha, T.; Selvin, P. R. Single-Molecule High-Resolution Imaging With Photobleaching. *Proc. Natl. Acad. Sci. U.S.A.* **2004**, *101*, 6462–6465.
- Qu, X. H.; Wu, D.; Mets, L.; Scherer, N. F. Nanometer-Localized Multiple Single-Molecule Fluorescence Microscopy. *Proc. Natl. Acad. Sci. U.S.A.* **2004**, *101*, 11298–11303.
- Balci, H.; Ha, T.; Sweeney, H. L.; Selvin, P. R. Interhead Distance Measurements in Myosin VI Via SHIRIMP Support a Simplified Hand-Over-Hand Model. *Biophys. J.* **2005**, *89*, 413–417.
- Förster, T. Energiewanderung Und Fluoreszenz. *Naturwissenschaften* **1946**, *6*, 166–175.
- Deniz, A. A.; Dahan, M.; Grunwell, J. R.; Ha, T.; Faulhaber, A. E.; Chemla, D. S.; Weiss, S.; Schultz, P. G. Single-Pair Fluorescence Resonance Energy Transfer on Freely Diffusing Molecules: Observation of Förster Distance Dependence and Subpopulations. *Proc. Natl. Acad. Sci. U.S.A.* **1999**, *96*, 3670–3675.
- Norman, D. G.; Grainger, R. J.; Uhrin, D.; Lilley, D. M. Location of Cyanine-3 on Double-Stranded DNA: Importance for Fluorescence Resonance Energy Transfer Studies. *Biochemistry* **2000**, *39*, 6317–6324.
- Iqbal, A.; Arslan, S.; Okumus, B.; Wilson, T. J.; Giraud, G.; Norman, D. G.; Ha, T.; Lilley, D. M. Orientation Dependence in Fluorescent Energy Transfer Between Cy3 and Cy5 Terminally Attached to Double-Stranded Nucleic Acids. *Proc. Natl. Acad. Sci. U.S.A.* **2008**, *105*, 11176–11181.
- Yang, C. H.; Soll, D. Studies of Transfer RNA Tertiary Structure of Singlet-Singlet Energy Transfer. *Proc. Natl. Acad. Sci. U.S.A.* **1974**, *71*, 2838–2842.
- Suddath, F. L.; Quigley, G. J.; McPherson, A.; Sneden, D.; Kim, J. J.; Kim, S. H.; Rich, A. Three-Dimensional Structure of Yeast Phenylalanine Transfer RNA at 3.0 Angstroms Resolution. *Nature* **1974**, *248*, 20–24.
- Ha, T.; Zhuang, X.; Kim, H. D.; Orr, J. W.; Williamson, J. R.; Chu, S. Ligand-Induced Conformational Changes Observed in Single RNA Molecules. *Proc. Natl. Acad. Sci. U.S.A.* **1999**, *96*, 9077–9082.
- Zhuang, X.; Bartley, L. E.; Babcock, H. P.; Russell, R.; Ha, T.; Herschlag, D.; Chu, S. A Single-Molecule Study of RNA Catalysis and Folding. *Science* **2000**, *288*, 2048–2051.
- Ditzler, M. A.; Aleman, E. A.; Rueda, D.; Walter, N. G. Focus on Function: Single Molecule RNA Enzymology. *Biopolymers* **2007**, *87*, 302–316.
- Cornish, P. V.; Ermolenko, D. N.; Staple, D. W.; Hoang, L.; Hickerson, R. P.; Noller, H. F.; Ha, T. Following Movement of the L1 Stalk Between Three Functional States in Single Ribosomes. *Proc. Natl. Acad. Sci. U.S.A.* **2009**, *106*, 5448.
- Ha, T. Single-Molecule Fluorescence Resonance Energy Transfer. *Methods* **2001**, *25*, 78–86.
- Jossinet, F.; Ludwig, T. E.; Westhof, E. RNA Structure: Bioinformatic Analysis. *Curr. Opin. Microbiol.* **2007**, *10*, 279–285.
- Beckert, B.; Nielsen, H.; Einvik, C.; Johansen, S. D.; Westhof, E.; Masquida, B. Molecular Modelling of the GIR Branching Ribozyme Gives New Insight into Evolution of Structurally Related Ribozymes. *EMBO J.* **2008**, *27*, 667–678.
- Hendrix, R. W. Symmetry Mismatch and DNA Packaging in Large Bacteriophages. *Proc. Natl. Acad. Sci. U.S.A.* **1978**, *75*, 4779–4783.
- Oram, M.; Sabanayagam, C.; Black, L. W. Modulation of the Packaging Reaction of Bacteriophage T4 Terminase by DNA Structure. *J. Mol. Biol.* **2008**, *381*, 61–72.

29. Casjens, S. R.; Gilcrease, E. B.; Winn-Stapley, D. A.; Schicklmaier, P.; Schmieger, H.; Pedulla, M. L.; Ford, M. E.; Houtz, J. M.; Hatfull, G. F.; Hendrix, R. W. The Generalized Transducing *Salmonella* Bacteriophage ES18: Complete Genome Sequence and DNA Packaging Strategy. *J. Bacteriol.* **2005**, *187*, 1091–1104.
30. Kemp, P.; Gupta, M.; Molineux, I. J. Bacteriophage T7 DNA Ejection into Cells Is Initiated by an Enzyme-Like Mechanism. *Mol. Microbiol.* **2004**, *53*, 1251–1265.
31. Reid, R. J. D.; Bodley, J. W.; Anderson, D. Characterization of the Prohead-pRNA Interaction of Bacteriophage Phi29. *J. Biol. Chem.* **1994**, *269*, 5157–5162.
32. Garver, K.; Guo, P. Boundary of pRNA Functional Domains and Minimum pRNA Sequence Requirement for Specific Connector Binding and DNA Packaging of Phage Phi29. *RNA* **1997**, *3*, 1068–1079.
33. Zhang, C. L.; Lee, C.-S.; Guo, P. The Proximate 5' and 3' Ends of the 120-Base Viral RNA (pRNA) Are Crucial for the Packaging of Bacteriophage  $\Phi$ 29 DNA. *Virology* **1994**, *201*, 77–85.
34. Reid, R. J. D.; Bodley, J. W.; Anderson, D. Identification of Bacteriophage Phi29 Prohead RNA (pRNA) Domains Necessary for *in Vitro* DNA-Gp3 Packaging. *J. Biol. Chem.* **1994**, *269*, 9084–9089.
35. Reid, R. J. D.; Zhang, F.; Benson, S.; Anderson, D. Probing the Structure of Bacteriophage Phi29 Prohead RNA With Specific Mutations. *J. Biol. Chem.* **1994**, *269*, 18656–18661.
36. Chen, C.; Sheng, S.; Shao, Z.; Guo, P. A Dimer As a Building Block in Assembling RNA: A Hexamer That Gears Bacterial Virus Phi29 DNA-Translocating Machinery. *J. Biol. Chem.* **2000**, *275*, 17510–17516.
37. Guo, S.; Tschammer, N.; Mohammed, S.; Guo, P. Specific Delivery of Therapeutic RNAs to Cancer Cells Via the Dimerization Mechanism of Phi29 Motor PRNA. *Hum. Gene Ther.* **2005**, *16*, 1097–1109.
38. Khaled, A.; Guo, S.; Li, F.; Guo, P. Controllable Self-Assembly of Nanoparticles for Specific Delivery of Multiple Therapeutic Molecules to Cancer Cells Using RNA Nanotechnology. *Nano Lett.* **2005**, *5*, 1797–1808.
39. Hoeprich, S.; Guo, P. Computer Modeling of Three-Dimensional Structure of DNA-Packaging RNA(prNA) Monomer, Dimer, and Hexamer of Phi29 DNA Packaging Motor. *J. Biol. Chem.* **2002**, *277*, 20794–20803.
40. Garver, K.; Guo, P. Mapping the Inter-RNA Interaction of Phage Phi29 by Site-Specific Photoaffinity Crosslinking. *J. Biol. Chem.* **2000**, *275*, 2817–2824.
41. Chen, C.; Guo, P. Magnesium-Induced Conformational Change of Packaging RNA for Procapsid Recognition and Binding During Phage Phi29 DNA Encapsidation. *J. Virol.* **1997**, *71*, 495–500.
42. Mohammad, T.; Chen, C.; Guo, P.; Morrison, H. Photoinduced Cross-Linking of RNA by Cis-Rh(Phen)2Cl2<sup>+</sup> and Cis-Rh(Phen)(Phi)Cl2<sup>+</sup>: a New Family of Light Activatable Nucleic Acid Cross-Linking Agents. *Bioorg. Med. Chem. Lett.* **1999**, *9*, 1703–1708.
43. Mat-Arip, Y.; Garver, K.; Chen, C.; Sheng, S.; Shao, Z.; Guo, P. Three-Dimensional Interaction of Phi29 pRNA Dimer Probed by Chemical Modification Interference, Cryo-AFM, and Cross-Linking. *J. Biol. Chem.* **2001**, *276*, 32575–32584.
44. Trottier, M.; Mat-Arip, Y.; Zhang, C.; Chen, C.; Sheng, S.; Shao, Z.; Guo, P. Probing the Structure of Monomers and Dimers of the Bacterial Virus Phi29 Hexamer RNA Complex by Chemical Modification. *RNA* **2000**, *6*, 1257–1266.
45. Chen, C.; Zhang, C.; Guo, P. Sequence Requirement for Hand-in-Hand Interaction in Formation of pRNA Dimers and Hexamers to Gear Phi29 DNA Translocation Motor. *RNA* **1999**, *5*, 805–818.
46. Zhang, C. L.; Tellinghuisen, T.; Guo, P. Confirmation of the Helical Structure of the 5'/3' Termini of the Essential DNA Packaging PRNA of Phage  $\Phi$ 29. *RNA* **1995**, *1*, 1041–1050.
47. Shu, D.; Moll, W. D.; Deng, Z.; Mao, C.; Guo, P. Bottom-Up Assembly of RNA Arrays and Superstructures As Potential Parts in Nanotechnology. *Nano Lett.* **2004**, *4*, 1717–1723.
48. Zhang, C. L.; Tellinghuisen, T.; Guo, P. Use of Circular Permutation to Assess Six Bulges and Four Loops of DNA-Packing PRNA of Bacteriophage Phi29. *RNA* **1997**, *3*, 315–322.
49. Wichitwechkarn, J.; Johnson, D.; Anderson, D. Mutant Prohead RNAs in the *in Vitro* Packaging of Bacteriophage Phi 29 DNA-Gp3. *J. Mol. Biol.* **1992**, *223*, 991–998.
50. Zhang, C. L.; Garver, K.; Guo, P. Inhibition of Phage Phi29 Assembly by Antisense Oligonucleotides Targeting Viral PRNA Essential for DNA Packaging. *Virology* **1995**, *211*, 568–576.
51. Trottier, M.; Garver, K.; Zhang, C.; Guo, P. DNA-Packaging pRNA As Target for Complete Inhibition of Viral Assembly *in Vitro* and *in Vivo*. *Nucleic Acids Symp. Ser.* **1997**, *36*, 187–189.
52. Zhang, H.; Shu, D.; Browne, M.; Guo, P. Approaches for Stoichiometry and Distance Determination of Nanometer Bio-Complex by Dual-Channel Single Molecule Imaging. *IEEE/NIH Life Sci. Syst. Appl. Workshop* **2009**, 124.
53. Zhang, H.; Shu, D.; Browne, M.; Guo, P. Construction of a Laser Combiner for Dual Fluorescent Single Molecule Imaging of pRNA of Phi29 DNA Packaging Motor. *Biomed. Microdevices* **2010**, *12*, 97–106.
54. Lakowicz, J. R. *Principles of Fluorescence Spectroscopy*, 3rd ed.; Springer Science+Business Media, LLC: New York, 2006.
55. Cherny, D. I.; Eperon, I. C.; Bagshaw, C. R. Probing Complexes With Single Fluorophores: Factors Contributing to Dispersion of FRET in DNA/RNA Duplexes. *Eur. Biophys. J.* **2009**, *38*, 395–405.
56. Lee, N. K.; Kapanidis, A. N.; Wang, Y.; Michalet, X.; Mukhopadhyay, J.; Ebright, R. H.; Weiss, S. Accurate FRET Measurements Within Single Diffusing Biomolecules Using Alternating-Laser Excitation. *Biophys. J.* **2005**, *88*, 2939–2953.
57. Ishii, Y.; Yoshida, T.; Funatsu, T.; Wazawa, T.; Yanagida, T. Fluorescence Resonance Energy Transfer Between Single Fluorophores Attached to a Coiled-Coil Protein in Aqueous Solution. *Chem. Phys.* **1999**, *247*, 163–173.
58. Woodson, S. A. Compact Intermediates in RNA Folding. *Annu. Rev. Biophys.* **2010**, *39*, 61–77.
59. Broyde, S.; Hingerty, B. 'A' Forms of RNAs in Single Strands, Duplexes and RNA-DNA Hybrids. *Nucleic Acids Res.* **1978**, *5*, 2729–2741.
60. Horton, N. C.; Finzel, B. C. The Structure of an RNA/DNA Hybrid: a Substrate of the Ribonuclease Activity of HIV-1 Reverse Transcriptase. *J. Mol. Biol.* **1996**, *264*, 521–533.
61. Guo, P.; Zhang, C.; Chen, C.; Trottier, M.; Garver, K. Inter-RNA Interaction of Phage Phi29 pRNA to Form a Hexameric Complex for Viral DNA Transportation. *Mol. Cell* **1998**, *2*, 149–155.
62. Chen, C.; Trottier, M.; Guo, P. New Approaches to Stoichiometry Determination and Mechanism Investigation on RNA Involved in Intermediate Reactions. *Nucleic Acids Symp. Ser.* **1997**, *36*, 190–193.
63. Trottier, M.; Guo, P. Approaches to Determine Stoichiometry of Viral Assembly Components. *J. Virol.* **1997**, *71*, 487–494.
64. Guo, P.; Grimes, S.; Anderson, D. A Defined System for *in Vitro* Packaging of DNA-Gp3 of the *Bacillus Subtilis* Bacteriophage Phi29. *Proc. Natl. Acad. Sci. U.S.A.* **1986**, *83*, 3505–3509.
65. Trottier, M.; Zhang, C. L.; Guo, P. Complete Inhibition of Virion Assembly *in Vivo* With Mutant PRNA Essential for Phage Phi29 DNA Packaging. *J. Virol.* **1996**, *70*, 55–61.
66. Guo, P.; Rajogopal, B.; Anderson, D.; Erickson, S.; Lee, C.-S. sRNA of Bacteriophage Phi29 of *B. Subtilis* Mediates DNA Packaging of Phi29 Proheads Assembled in *E. Coli*. *Virology* **1991**, *185*, 395–400.
67. Lee, C. S.; Guo, P. *In Vitro* Assembly of Infectious Virions of Ds-DNA Phage  $\Phi$ 29 From Cloned Gene Products and Synthetic Nucleic Acids. *J. Virol.* **1995**, *69*, 5018–5023.
68. Clegg, R. M.; Murchie, A. I. H.; Zechel, A.; Lilley, D. M. J. Observing the Helical Geometry of Double-Stranded Dna in Solution by Fluorescence Resonance Energy-Transfer. *Proc. Natl. Acad. Sci. U.S.A.* **1993**, *90*, 2994–2998.
69. Wozniak, A. K.; Schroder, G. F.; Grubmuller, H.; Seidel, C. A.;

- Oesterhelt, F. Single-Molecule FRET Measures Bends and Kinks in DNA. *Proc. Natl. Acad. Sci. U.S.A.* **2008**, *105*, 18337–18342.
70. Zhang, C. L.; Trottier, M.; Guo, P. X. Circularly Permuted Viral prRNA Active and Specific in the Packaging of Bacteriophage  $\Phi$ 29 DNA. *Virology* **1995**, *207*, 442–451.
71. Pan, T.; Gutell, R. R.; Uhlenbeck, O. C. Folding of Circularly Permuted Transfer RNAs. *Science* **1991**, *254*, 1361–1364.
72. Nolan, J. M.; Burke, D. H.; Pace, N. R. Circularly Permuted tRNAs As Specific Photoaffinity Probes of Ribonuclease P RNA Structure. *Science* **1993**, *261*, 762–765.
73. Liu, H.; Guo, S.; Roll, R.; Li, J.; Diao, Z.; Shao, N.; Riley, M. R.; Cole, A. M.; Robinson, J. P.; Snead, N. M.; et al. Phi29 pRNA Vector for Efficient Escort of Hammerhead Ribozyme Targeting Survivin in Multiple Cancer Cells. *Cancer Biol. Ther.* **2007**, *6*, 697–704.
74. Li, N.; Yu, C.; Huang, F. Novel Cyanine-AMP Conjugates for Efficient 5' RNA Fluorescent Labeling by One-Step Transcription and Replacement of [ $\gamma$ -32P]ATP in RNA Structural Investigation. *Nucleic Acids Res.* **2005**, *33*, e37.
75. Phillips, J. C.; Braun, R.; Wang, W.; Gumbart, J.; Tajkhorshid, E.; Villa, E.; Chipot, C.; Skeel, R. D.; Kale, L.; Schulten, K. Scalable Molecular Dynamics With NAMD. *J. Comput. Chem.* **2005**, *26*, 1781–1802.
76. Foloppe, N.; MacKerell, A. D. All-Atom Empirical Force Field for Nucleic Acids: I. Parameter Optimization Based on Small Molecule and Condensed Phase Macromolecular Target Data. *J. Comput. Chem.* **2000**, *21*, 86–104.
77. MacKerell, A. D.; Banavali, N. K. All-Atom Empirical Force Field for Nucleic Acids: II. Application to Molecular Dynamics Simulations of DNA and RNA in Solution. *J. Comput. Chem.* **2000**, *21*, 105–120.
78. Harris, S.; Schroeder, S. J. Nuclear Magnetic Resonance Structure of the Prohead RNA E-Loop Hairpin. *Biochemistry* **2010**, *49*, 5989–5997.
79. Xiao, F.; Zhang, H.; Guo, P. Novel Mechanism of Hexamer Ring Assembly in Protein/RNA Interactions Revealed by Single Molecule Imaging. *Nucleic Acids Res.* **2008**, *36*, 6620–6632.
80. Guo, P. Structure and Function of Phi29 Hexameric RNA That Drive Viral DNA Packaging Motor: Review. *Prog. Nucleic Acid Res. Mol. Biol.* **2002**, *72*, 415–472.
81. Zhang, C.; Trottier, M.; Chen, C.; Guo, P. Chemical Modification Patterns of Active and Inactive As Well As Procapsid-Bound and Unbound DNA-Packaging RNA of Bacterial Virus Phi29. *Virology* **2001**, *281*, 281–293.
82. Huang, F. Efficient Incorporation of CoA, NAD and FAD into RNA by In Vitro Transcription. *Nucleic Acids Res.* **2003**, *31*, e8.